AD-A091 759 CAMBRIDGE UNIV (ENGLAND) DEPT OF METALLURGY AND MAT--ETC F/G 20/11
MICROHARDNESS, FRICTION AND WEAR OF SIC AND SI3N4 MATERIALS AS --ETC(U)
OCT 79 M G NAYLOR, T F PAGE DA-ERO-78-G-010

UNCLASSIFIED NL

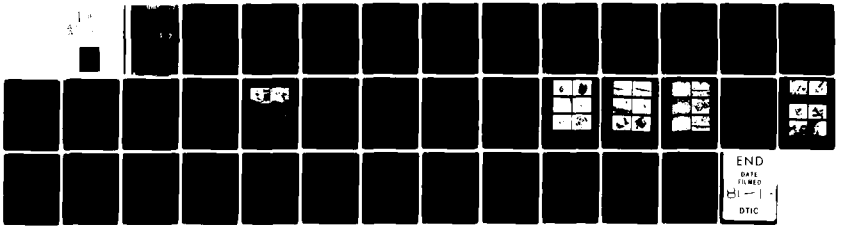

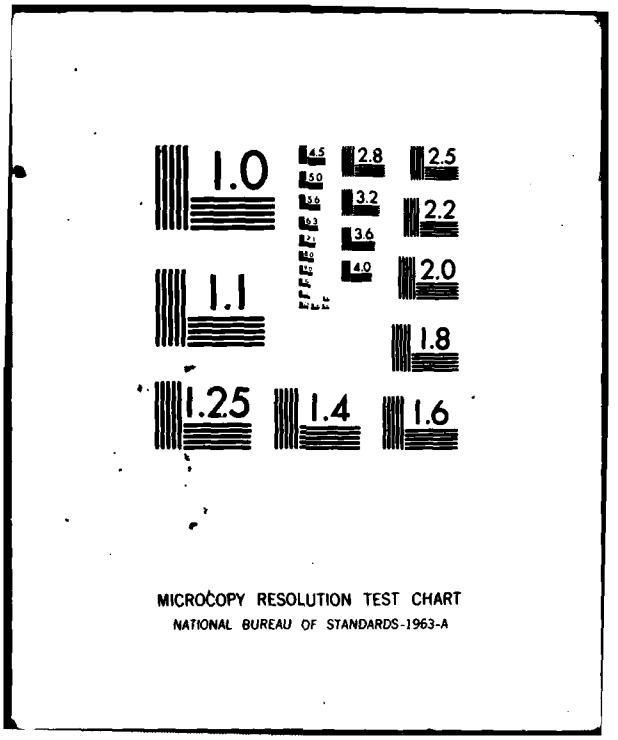
1.0
1.1
1.25
1.4
1.6
1.8
2.0
2.2
2.5
2.8
3.2
3.6
4.0
4.5
5.0
5.6
6.3
MICROCOPY RESOLUTION TEST CHART
NATIONAL BUREAU OF STANDARDS-1963-A

AD A091759

[illegible] AND [illegible]
[illegible] AS A [illegible]
[illegible] AND [illegible]

FIRST ANNUAL TECHNICAL REPORT

By

M.G.S. Naylor and T.F. Page

October 1979

DTIC
ELECTE
NOV 1 8 1980
S D
E

EUROPEAN RESEARCH OFFICE
United States Army,
London, NW1 5TH,
England.

GRANT NUMBER DA-ERO-78-G-010

University of Cambridge,
England.

Approved for Public Release: distribution unlimited

80 11 [illegible]

SECURITY CLASSIFICATION OF THIS PAGE (When Data Entered)

REPORT DOCUMENTATION PAGE

READ INSTRUCTIONS BEFORE COMPLETING FORM

1. REPORT NUMBER

2. GOVT ACCESSION NO. AD-A091 759

3. RECIPIENT'S CATALOG NUMBER

4. TITLE (and Subtitle)

MICROHARDNESS, FRICTION AND WEAR OF SiC AND Si_3N_4 MATERIALS AS A FUNCTION OF LOAD, TEMPERATURE AND ENVIRONMENT.

5. TYPE OF REPORT & PERIOD COVERED

Annual Technical Report, 1 October 78 — 30 Sept 79

6. PERFORMING ORG. REPORT NUMBER

7. AUTHOR(s)

M.G.S. Naylor and T.F. Page

8. CONTRACT OR GRANT NUMBER(s)

DAERO-78-G-010

9. PERFORMING ORGANIZATION NAME AND ADDRESS

Department of Metallurgy and Materials Science,
University of Cambridge,
Cambridge, CB2 3QZ, U.K.

10. PROGRAM ELEMENT, PROJECT, TASK AREA & WORK UNIT NUMBERS

11. CONTROLLING OFFICE NAME AND ADDRESS

12. REPORT DATE

October 1979

13. NUMBER OF PAGES

33

14. MONITORING AGENCY NAME & ADDRESS (if different from Controlling Office)

38

15. SECURITY CLASS. (of this report)

UNCLASSIFIED

15a. DECLASSIFICATION/DOWNGRADING SCHEDULE

16. DISTRIBUTION STATEMENT (of this Report)

Approved for public release: distribution unlimited.

17. DISTRIBUTION STATEMENT (of the abstract entered in Block 20, if different from Report)

18. SUPPLEMENTARY NOTES

19. KEY WORDS (Continue on reverse side if necessary and identify by block number)

Ceramic, silicon carbide, silicon nitride, single crystal SiC, hot-pressed SiC, sintered SiC, reaction-bonded SiC, pyrolytically-deposited Si_3N_4, hardness, microhardness, temperature dependence of hardness, indentation plasticity, indentation fracture, fracture toughness, load sensitivity of hardness, indentation size effect.

20. ABSTRACT (Continue on reverse side if necessary and identify by block number)

See over

DD FORM 1 JAN 73 1473 EDITION OF 1 NOV 65 IS OBSOLETE

UNCLASSIFIED

SECURITY CLASSIFICATION OF THIS PAGE(When Data Entered)

As part of the overall research program aimed at an investigation of the hardness, friction and wear behaviour of SiC and Si_3N_4 engineering ceramics as a function of load, temperature and environment, the microhardness and indentation fracture response of various forms of SiC (1) and one form of Si_3N_4 have been studied using both Vickers and Knoop indentation techniques at temperatures ranging from 20-800°C and at applied loads of between 0.1 and 1kgf, in vacuo.

Lateral fracture around Knoop indentations has been found to increase markedly with temperature for single crystal (0001), hot-pressed and reaction-bonded silicon carbides, although not for sintered SiC. The Knoop hardness of all these materials decreased by a factor of ∿2 over the temperature range investigated (2300kgfmm^{-2} at room temperature; 1200kgfmm^{-2} at 800°C for hot-pressed SiC), whilst corresponding Vickers hardness values typically decreased by a factor of ∿3 over the range (2800kgfmm^{-2} at room temperature; 1000kgfmm^{-2} at 800°C for hot-pressed SiC). Different microstructural forms of SiC were found to have different hardness/temperature responses.

Pyrolytically-deposited Si_3N_4 (PDSN) showed a much smaller dependence of hardness on temperature, the Vickers hardness changing linearly from 3000kgfmm^{-2} at room temperature to 2100kgfmm^{-2} at 800°C.

Indentation fracture mechanics analyses (in terms of K_c, P* and c*) have been performed for median cracks around Vickers indentations in hot-pressed and single crystal SiC and for PDSN, again as a function of temperature. All three materials showed a decrease in K_c with increasing temperature (though the forms of the decrease differed). Crack initiation (quantified by P* and c*) became easier with increasing temperature in the case of (0001) single crystal SiC, more difficult in the case of hot-pressed SiC, but remained invariant in the case of PDSN.

In all cases, examination of indented samples (by both optical and SEM methods) has been used to establish the microstructural control of indentation fracture paths and surface deformation structures etc.

Accession For
NTIS GRA&I
DDC TAB
Unannounced
Justification
By
Distribution/
Availability Codes
Dist | Avail and/or special
A

CONTENTS PAGE

1. INTRODUCTION

Engineering ceramics based on SiC and Si_3N_4 have been developed primarily for high temperature applications such as gas turbine components (e.g. 2,3), but have also found increasing utilization as bearing and abrasion-resistant surfaces (2-5) due to their excellent (unlubricated) friction and wear characteristics. It is this latter area of utilization which is of primary interest to the present program of research, though most of the results on microstructural characterization and control of deformation behaviour etc. are of much wider significance to the general behaviour of SiC and Si_3N_4 ceramics.

Material loss in abrasive and erosive situations is controlled by some combination of fundamental deformation mechanisms, such as localized plasticity (e.g. 10) often coupled with a number of crack arrays in brittle solids (e.g. 11). These mechanisms are most conveniently investigated and quantified experimentally by means of indentation hardness tests, simple sliding stylus wear tests etc., and previous research* in Cambridge (e.g. 6-8) has characterized the basic deformation behaviour and microstructural control of such properties at room temperature under ambient conditions. Thus, several materials' microstructures have previously been evaluated (e.g. 70), hardness anisotropy and etching used to evaluate the slip response of SiC single crystals to hardness tests (e.g. 18, 74) and the indentation fracture behaviour and microstructural control of crack paths examined in a range of SiC and Si_3N_4 ceramics (6-8) - all at room temperature. Non-ERO-supported investigations in Cambridge have made parallel studies of the load dependence of hardness in brittle solids (18, 20) and the role of phase transformations in the microstructural development of SiC (81).

Thus the aim of the current program is to significantly extend these investigations to include important variables such as temperature and environment, by utilizing a variety of indentation and sliding stylus test techniques performed in a controlled-atmosphere, temperature-variable microhardness tester commissioned especially for this project (1,9). In parallel with these investigations a wide range of optical, electron optical (SEM, TEM, STEM) and X-ray diffraction techniques are being utilized for the characterization of specimen microstructures and both surface and subsurface contact-induced deformation structures.

The types of information which may be derived from such hardness experiments etc. are reviewed in sections 2 (indentation plasticity) and 3 (indentation fracture), with a review of existing literature on the temperature dependence of these mechanisms presented in section 4.

---

* Also supported by the European Research Office of the U.S. Army 1973-76 (e.g. 82).

2. INDENTATION PLASTICITY

It has been established by a variety of techniques (e.g. TEM, etch pitting, cathodoluminescence, selected area electron channelling) that even the most brittle materials exhibit some form of slip response, however localized, to surface contact situations involving sharp indenters, e.g. Vickers or Knoop hardness indentations, abrasive wear tracks or erosive impacts (e.g. 6-8, 10, 12-14). This is a consequence of the large localized shear stresses produced in such situations (e.g. 7, 8, 15), together with local hydrostatic compression (which inhibits massive cracking) and tensile stresses (which can cause arrested growth of a number of crack geometries - see section 3).

Solutions for the elastic stress fields beneath blunt (Hertzian) and sharp (Boussinesq) indenters have been obtained (see, for example, (32)), but elastic/plastic indentation stress fields have not yet been completely characterized (80). However, the most widely-adopted model for the effects of the plastic zone in modifying sub-indentation stress fields is the spherical cavity model due to Hill (78, 18). Further, Evans (80) has coupled the elastic and elastic/plastic solutions, predicting a peak in the tensile stress at the elastic/plastic boundary and enabling residual stresses after indenter removal to be considered. Additionally, Evans (80) has performed a finite difference calculation for rigid-sphere indentation which predicts plastic zone shapes and sizes (also maximum tensile stress values) in broad agreement with analytic solutions and experimental observations by the techniques listed above.

In the case of SiC materials, the depth of the plastic zone has been estimated from selected-area electron channelling data to be 5.5 times the indentation radius (a) (14), whilst the surface plastic zone radius has been investigated by chemical etching (74) which produces only a very local change in indentation shapes, with no evidence of dislocation etch pits extending into the material. This is consistent with etching, cathodoluminescence and slip line observations on a wide range of ceramic materials by Evans and Wilshaw (35), indicating a surface plastic region of radius $\sim$1.1-1.3a only. TEM observations of this plastic zone (associated with wear tracks) have also been made (e.g. 6).

The precise role of plasticity in surface contact situations has yet to be established, although, from previous work in Cambridge (16), it has been conjectured that (in highly brittle materials) the role of slip may be in accommodating material displaced by other deformation mechanisms such as elasticity, microfracture and possibly block shear or even densification (specifically in materials with the zinc-blende structure, such as β-SiC (e.g. 16-18)). Despite this uncertainty, plasticity models have been successfully invoked to explain a number of indentation phenomena such as single crystal hardness anisotropy (e.g. 19) and load sensitivity of hardness (e.g. 18,20), as well as to derive hardness/plastic yield stress relationships for brittle solids (e.g. 21-23).

Probably the most important experimental use of indentation plasticity is in the determination of slip geometries from hardness anisotropy measurements on single crystals by considering the effective

resolved shear stresses on the crystallographic slip system array beneath the indenter (19,24). This approach has been used on a wide range of materials (e.g. 24), especially on otherwise brittle solids such as transition metal carbides (25-28) as well as SiC (8, 16, 19, 29) and Si_3N_4 (30). The latter results are of particular interest in the present investigation: room temperature slip systems have been determined as $\{1\bar{1}00\}\langle 11\bar{2}0\rangle$ and $\{0001\}\langle 11\bar{2}0\rangle$ for different indenter orientations on α-SiC single crystal (16), and as $\{1\bar{1}00\}[0001]$ from room temperature to 1500°C in the case of α-Si_3N_4 single crystal (30).

As well as the applications described above, indentation plasticity is thought to play a significant role in crack genesis during indentation fracture beneath sharp indenters (e.g. 31), and this is further discussed in the following section.

Various aspects of indentation plasticity in SiC and Si_3N_4 were investigated as part of the previous ERO-supported program (e.g. hardness anisotropy (16), etching behaviour (74) and the occurrence of plasticity during response to simple wear tests (6-8)).

3. INDENTATION FRACTURE

Indentation fracture geometries have been characterized and modelled principally by Lawn, Evans and co-workers (e.g. 32-35): in the case of sharp surface contact, cracks perpendicular to the specimen surface (median cracks) are created during loading, cracks approximately parallel to the test surface (lateral cracks) being created during unloading. More complex geometries (such as radial cracks which may form on loading or unloading or both) have also been observed (35-38). The precise sequence of microfracture events in the indentation process is open to question (14), but it would appear that radial cracks are the first to form beneath Vickers indentations in SiC (14,35), depending on applied load and surface preparation (35).

It has been established that the incidence of lateral fracture in particular (35), combined with other crack types, plays a dominant role in the abrasive and erosive wear of brittle materials, and that with increasing load, a transition from plasticity control to fracture control of abrasive wear is observed (39).

The microstructural dependence of indentation fracture, in terms of preferred fracture paths, may easily be investigated by direct examination of indentations in a range of materials, enabling conclusions to be drawn as to materials response to abrasive environments and this has been one of the principal interests of the authors and co-workers (6-8).

A quantitative fracture mechanics model for the dependence of crack extent on contact load has been developed (40-42) by considering the interaction of the tensile component of the sub-indentation stress field with pre-existing flaws within the test material. For median crack propagation, the following relationship was obtained:

a) $(P/c)^{3/2} = \beta_o K_c$ (for explanation of terms, see glossary) where $\beta_o \sim 7$

For initiation of median fracture, the following critical load and pre-existing flaw size parameters were derived in an 'index of brittleness' approach:

b) $P^* = \lambda_o (K_c/H)^3 K_c$ where λ_o is estimated to be $\sim 2.2 \times 10^4$

c) $c^* = \mu_o (K_c/H)^2$ where μ_o is estimated to be ~ 44.2

Lawn and Marshall (42) have modified the coefficients in the above equations to fit a wide range of experimental data, giving $\lambda_o \sim 1.6 \times 10^4$; $\mu_o \sim 120$, which are the coefficients used in the present analysis. It should be recognized that the theory involves many assumptions and approximations (41, 42) which render the absolute results accurate to within approximately an order of magnitude only. However, direct measurements of P^* and c^* on a range of materials by Lankford and Davidson (43), using a combination of SEM and acoustic emission techniques, indicate fair agreement between actual behaviour and theory.

The effects of the sub-indentation plastic zone in modifying the stress fields, and hence fracture behaviour, have been discussed in detail by Evans (80). In summary, it is observed that at small (c/a)

values, the local elastic/plastic field dominates the fracture behaviour (especially for materials of low hardness) and the Palmqvist relationship Pαc holds. At higher ($^c/_a$) values (obtained experimentally by merely increasing the applied load), especially for relatively hard materials, the Lawn and Evans model (41) holds and $Pαc^{3/2}$ - in this case the fracture is largely within the elastic region, and plastic zone effects are minimal. Evans (80) has introduced a further function g_2 (obtained empirically) to incorporate effects due to the plastic zone radius:

$$\text{(d)} \quad \frac{K_c}{H\sqrt{a}} = g_1\,(^c/_a)\; g_2(^E/_H)$$

where

$$\text{(e)} \quad g_1\,(^c/_a) = (^c/_a)^{-1/2} \quad \text{for Palmqvist case}$$

$$\text{(f)} \quad g_1\,(^c/_a) = (^c/_a)^{-3/2} \quad \text{for Lawn/Evans case}$$

) with $g_2 = 1$

and

$$\text{(g)} \quad g_2(^E/_H) = (E/H)^{2/5} \quad \text{(for best correlation with data).}$$

The introduction of g_2 enables a universal indentation fracture curve to be drawn over the whole ($^c/_a$) range for all materials. However the precise form of $g_1(^c/_a)$ must then be determined by best fit to this universal curve. Effects due to Poisson's ratio variation and indenter friction have also been discussed, but not quantified, by Evans (80).

Recently, Hagan (31) has produced a model for median crack nucleation by dislocation pile-up in crystalline materials, or intersection of shear lines in glasses (79), which does not require the assumption of pre-existing flaws, and which predicts values of P* substantially lower than those of Lawn et al. (by a factor of ∿18). Hagan's model also predicts nucleation and growth of cracks by the action of indentation plasticity mechanisms alone to sizes comparable with the critical dimensions(c*) required by Lawn et al. for subsequent propagation. The extent to which this effect competes with the influence of pre-existing flaw distributionsrequires further investigation, although nucleation centres in glass are found to be largely indentation-induced, with pre-existing flaws occasionally acting as nuclei (42). Radial crack nucleation in a range of materials has been found to be a function of surface finish (35) (indicating a marked dependence on pre-existing flaw distribution) but lateral cracks are observed to form, independently of surface preparation, in the vicinity of the elastic/plastic boundary (35), suggesting that deformation initiated (or extended) flaws are likely precursors in this case.

In summary, indentation techniques provide a useful (if theoretically complex), non-destructive experimental means of studying fracture in brittle materials or, for example, explaining strength degradation after surface contacts (44). Quantitative results for crack propagation and initiation may easily be obtained as a function of specimen microstructure, temperature, environment etc. In addition, such experiments are invaluable in allowing preferred fracture paths through specimen microstructures to be examined.

4. TEMPERATURE EFFECTS

Although most reported studies of microhardness behaviour have concerned experiments performed under ambient conditions, there have been several investigations of the effects of temperature for metals (e.g. 45-48) and ceramics (e.g. 48-63). In general, ceramic materials often display a marked decrease of hardness with temperature, frequently involving a "ductile-brittle" transition in the temperature range 0.2 - 0.5 T_m (51) (at given strain rates). The decrease in hardness may be explained in terms of increasing plasticity arising either from a diminution of the Peierls-Nabarro stress or from increased thermal diffusion of dislocation pinning mechanisms or from a change in active slip system(s) or some combination of these (e.g. 48, 51, 52).

This latter (slip system) effect is most conveniently investigated by means of single crystal hardness anisotropy experiments at various temperatures (e.g. 28, 30, 48, 53, 54). The most successful example of this technique has been the case of transition metal carbides (e.g. 28, 48, 51, 55-57), which are found to show three régimes of anisotropy behaviour, corresponding to {110}<110> slip system for the low-temperature régime, {111}<110>for the high-temperature range, and a combination of the two in the intermediate régime. This has been interpreted in terms of a transition in atomic cohesion from covalent bonding (low-temperature) to metallic bonding (high-temperature) (e.g. 26, 27).

In contrast, SiC and Si_3N_4 are far less 'metallic' in character and therefore retain their hardness to higher homologous temperatures (51). However, Trefilov et al. (58) have found the hot-hardness behaviour of single crystal SiC to be similar to that of Si, Ge and InSb, and have tentatively suggested that this is consistent with a pressure-induced metallic transformation, presumably occurring only in a very localized region beneath the indenter in the initial (very high contact pressure) stages of the indentation process (Sawyer et al.(16) discuss this aspect more fully). The available data suggests that such densification effects, whether widespread or not, are not reflected in a change in slip system with temperature, as in the above case. Thus Niihara and Hirai (30) have determined the active slip systems of single crystal α-Si_3N_4 to be $\{10\bar{1}0\}\langle 0001\rangle$ from room temperature to 1500°C (0.8T_m). However, while single crystal SiC has been examined at room temperature (16 - see section 2), high temperature Vickers hardness investigations by Hirai and Niihara (59) do not include sufficient indenter orientations for determination of slip systems, although the measured anisotropies remain constant from room temperature to 1500°C (0.6T_m).

Direct comparison of existing data on the hot hardness of SiC and Si_3N_4 materials is difficult, due to the wide range of experimental techniques used (e.g. dynamic (55, 60), mutual (51) and assorted diamond indentation techniques (30, 50, 58, 59)). Similarly, the sources, purities and microstructural states of the materials is unclear in virtually all cases. Hence there is a need for a systemmatic investigation of changes in hardness and indentation fracture behaviour of a range of microstructural states of the same material as a function of temperature (1).

To date, the only microstructural factor investigated as possibly influencing the temperature dependence of the hardness of ceramic

materials appears to be the effect of porosity (48, 51, 55, 61): for example, below 0.4 Tm, appreciable porosity (e.g. 20%) in TiC results in a lower hardness value whereas, at higher temperatures, hardness is found to be independent of porosity.

The variation of indentation fracture behaviour with temperature for brittle materials has not been widely reported except in the following cases. MgO has been found to exhibit marked cracking up to 800°C, "dislocation interaction cracks" between 800 and 1000°C with no fracture above 1000°C (48, 51). Dynamic hardness tests by Fitzgerald (55) have revealed an increase in the number of cleavage cracks in single crystal TiC with increasing temperature, and the onset of ring cracking in polycrystalline B_4C above 1340°C. Finally, single crystal SiC has been observed to exhibit an increase in indentation fracture (around Berkovich indentations) with temperature up to 800°C (58), but above this temperature the extent of radial fracture around Vickers indentations reportedly decreases (59). To the authors' knowledge, the present investigation represents the first attempt to quantify the variation of fracture with temperature by application of indentation fracture mechanics analyses.

The effects of temperature on frictional properties of various refractory materials (e.g. TiC, SiC, TiO, B_4C) have been studied by Brookes and co-workers (61-63), with the conclusion that the coefficient of friction (μ) is independent of both the onset of bulk plastic flow and the rapid decrease of hardness with increasing temperature, but may increase as a result of plastic deformation and diffusion acting together above $\sim 0.46\ T_m$(TiC). Adsorbed gases were also found to have a pronounced effect on μ(63).

The effects of adsorbed species, especially water, on hardness (and other) properties of ceramic materials is well-established (e.g. 64, 65): both softening and anomalous room temperature creep of surface layers is observed. For materials prone to such chemomechanical effects, thermal desorption of adsorbed species will result in changes in hardness behaviour in addition to the variations discussed above.

All experiments described here were performed in liquid nitrogen-trapped high vacuum ($<10^{-6}$mmHg) in order to eliminate these effects (particularly the effect of water) as far as possible.

5. EXPERIMENTAL

5.1 MATERIALS

The materials used in this investigation to date were commercially available forms of polycrystalline silicon carbides* plus a large (0001) single crystal SiC, together with a pyrolytically-deposited silicon nitride*(PDSN) sample (see table 1).

Sections of each of the polycrystalline samples were cut using a high-speed diamond saw (e.g. 70) and these, together with a selected as-grown basal habit single crystal SiC, were mounted in electrically-conducting resin and diamond lapped and polished to 0.25 μm finish (e.g. 9). Specimens were then examined optically and by SEM (uncoated, except for PDSN, for which a separate specimen was gold coated), porosity and residual Si contents being measured directly from optical images by a Quantimet 720B image analyzer (table 1). Notable micro-structural features are discussed below.

Two grades of reaction-bonded SiC (designated (a) and (b)), having slightly different grain sizes, were used. This form of SiC has ∿10-15 vol.% unreacted silicon forming an interconnected network through the material. A detailed characterization of 'REFEL' microstructures has been given (70, 9) but, with respect to the results and micrographs in section 6, it should be noted that secondary electron SEM images of polished, uncoated 'REFEL' show the following impurity-controlled (8, 70, 71) contrast effects: usually each SiC grain appears as a composite, comprising a (dark) angular core (the original grit seed) surrounded by a lighter imaging layer of epitaxial material of the same crystal structure formed from graphite and silicon during the reaction-bonding process. The remaining volume of unreacted silicon appears as dark, irregular areas. Optically, the silicon appears white and the SiC crystal array grey. No regions of fine β-SiC crystals (nucleated on the graphite (70)) were observed in the samples for this study.

The sintered and hot-pressed materials also show (much fainter) intergranular secondary electron SEM contrast which is believed to be impurity-controlled. In addition, the hot-pressed carbide (Norton NC203) has specular white intergranular particles, which energy-dispersive X-ray analysis (Link 860) has shown to contain large amounts of tungsten - presumably as WC.

---

* N.B. SiC displays a number of polytypic stacking sequences (66), one of which is cubic (β or 3C in Ramsdell notation), the rest being designated as α (hexagonal or rhombohedral) structures, the most common being 6H (67). Silicon nitride exists in two hexagonal crystalline polymorphs (α and β) (e.g. 68, 83, 84).

Material	Source	Main Polytype	Grain size	Porosity
(0001) single crystal SiC	Arendal Smelteverk (Norway)	α (Ref. 16)	-	-
Hot-Pressed SiC	Norton Co. U.S.A. (NC203)	α (Ref.7)	Bimodal (Ref.7): peaks at 0.6 and 1.6 μm	-
Sintered SiC	Carborundum Co. U.S.A.	α (*)	$\lesssim$ 10 μm	8 vol%
REFEL+ Reaction-bonded SiC	UKAEA, Springfields, U.K.	α (Ref.70)	(a) ∿10μm	None, but 14 vol.% unreacted Si
(two grades)		α	(b) ∿5μm	None, but 12 vol.% unreacted Si
Pyrolytically-deposited Si_3N_4	Admiralty Marine Technology Establishment, Holton Heath.	α (Ref.69)	∿ 50 μm (Ref.69)	Small amount (not measured)

* Carborundum Technical Data Sheet

+ 'REFEL' is a registered trade mark of UKAEA.

Table 1. Materials investigated.

5.2 INDENTATION TECHNIQUES

Hot-hardness experiments were carried out in a Wilberforce Scientific Developments (Coventry, U.K.) high temperature microhardness tester coupled to a four-inch oil diffusion pump with liquid nitrogen trapping (fig. 1). The instrument consists of specimen and indenter assemblies together with heating furnaces and water cooling systems contained in a sealed stainless steel vessel capable of evacuation to $\sim 2 \times 10^{-7}$ torr to 1×10^{-6} torr (with the furnaces outgassed and at temperature), with gas-bleed facilities for operating in controlled gaseous environments. All the experiments described here were performed 'in vacuo' to prevent furnace oxidation and indenter graphitization and to exclude (as far as possible) any environmental or Rebinder effects which are important in some ceramic materials (e.g. 64, 65).

Polished specimens were bonded to a stainless steel stub with a refractory aluminium orthophosphate cement which was cured at $\sim 300^{\circ}C$ for a few hours (9, 72). The stub, to which a chromel alumel thermocouple was spot-welded, was then screwed onto a pedestal in the bottom of the specimen furnace assembly within the instrument (fig. 1d).

The entire specimen assembly was capable of rotation and translation in orthogonal directions controlled by external micrometers. In the viewing position (fig. 1c), the specimen could be examined through a 1.8 mm quartz window by a Zeiss Epignost II microscope fitted with a Leitz long working distance objective lens and a screw micrometer measuring-eyepiece. Other than for viewing, the whole furnace unit could be translated to a position directly underneath the indenter assembly, which comprised a mechanically-retained diamond (Knoop or Vickers profile) on a stainless steel shank contained in its own separately-controlled furnace, and loaded by a series of weights stacked in a stepped cylinder. Winding this cylinder down resulted in progressively more weights being lowered onto a collar in the indenter shank. An external oil dashpot controlled the descent of the indenter, and various electrical contacts on the supporting double cantilever assembly enabled a constant loading time (15 seconds) to be used for each indentation.

Vickers and Knoop hot-hardness experiments were performed as in table 2, at loads of 100, 200, 500 and 1000gf (generally 5 indentations being used at each load), over the temperature ranges indicated (at $100^{\circ}C$ or $200^{\circ}C$ intervals, as required). At each temperature, half an hour (at least) was allowed for stabilization of indenter and specimen temperatures prior to indenting the specimen.

For the (0001) single crystal SiC, Knoop indentations were aligned such that the long axis was approximately parallel to a $\langle 11\bar{2}0 \rangle$ direction - the 'hardest' direction on (0001) (16,74). Vickers indentations were aligned so that one diagonal was parallel to this direction.

Besides being observed at temperature, indentations were subsequently examined and photographed both optically (Neophot II or Zeiss Universal) and by scanning electron microscopy (ISI 100A or Cambridge SIIA) as in section 5.1. The extent of lateral fracture around Knoop indentations was examined (for the carbides) and, using Vickers indentation data for (0001) single crystal SiC, hot-pressed SiC and PDSN, the variation of radial crack extent with load and temperature was analyzed as in

Material	Indenter	Temp. range - investigated
(0001) single crystal SiC	Knoop Vickers*	Room Temp. - 800°C Room Temp. & 800°C (only)
Hot-pressed SiC	Knoop Vickers*	Room Temp. - 800°C Room Temp. - 800°C
Sintered SiC	Knoop	Room Temp. - 800°C
Reaction-bonded SiC a) b)	Knoop Vickers	Room Temp. - 900°C Room Temp. - 800°C
Pyrolytically-deposited Si_3N_4	Vickers*	Room Temp. - 800°C

*Table 2. A summary of experimental work performed. *Indicates crack lengths were measured for indentation fracture mechanics analysis. Knoop indenter profiles generally promote lateral cracking whereas Vickers indentations usually exhibit pronounced radial fracture. Thus materials' responses to both Vickers and Knoop indentation processes may be used to completely characterize the susceptibility to indentation fracture.*

section 3. Firstly, the slope of the logc/logP plot(m) was determined in each case: a value of 2/3 indicating $Pac^{3/2}$ (the Lawn et al. case 41)), a value of 1 indicating Pac (the Palmqvist case (80)) - see section 3. Typically, m was found to lie between 0.6 and 0.75 (±0.03) and so the analysis due to Lawn and Evans (41) was used. For this, the slope of the $c^{3/2}$ versus P plot was determined using the method of least squares*. Using equation (a) (section 3), K_c values were derived from the gradients obtained at different temperatures, assuming β_o=7, and finally, values of P* and c* were calculated from K_c and the mean values of H over the load range in each case (H was found to be slightly load dependent in the load range used).

---

* This least squares fit should minimize the variances in the experimental observation $c^{3/2}$ NOT those in the fixed load P, and this was found to have a significant (∿20%) effect on the K_c values obtained and a larger (80%) effect on P*.

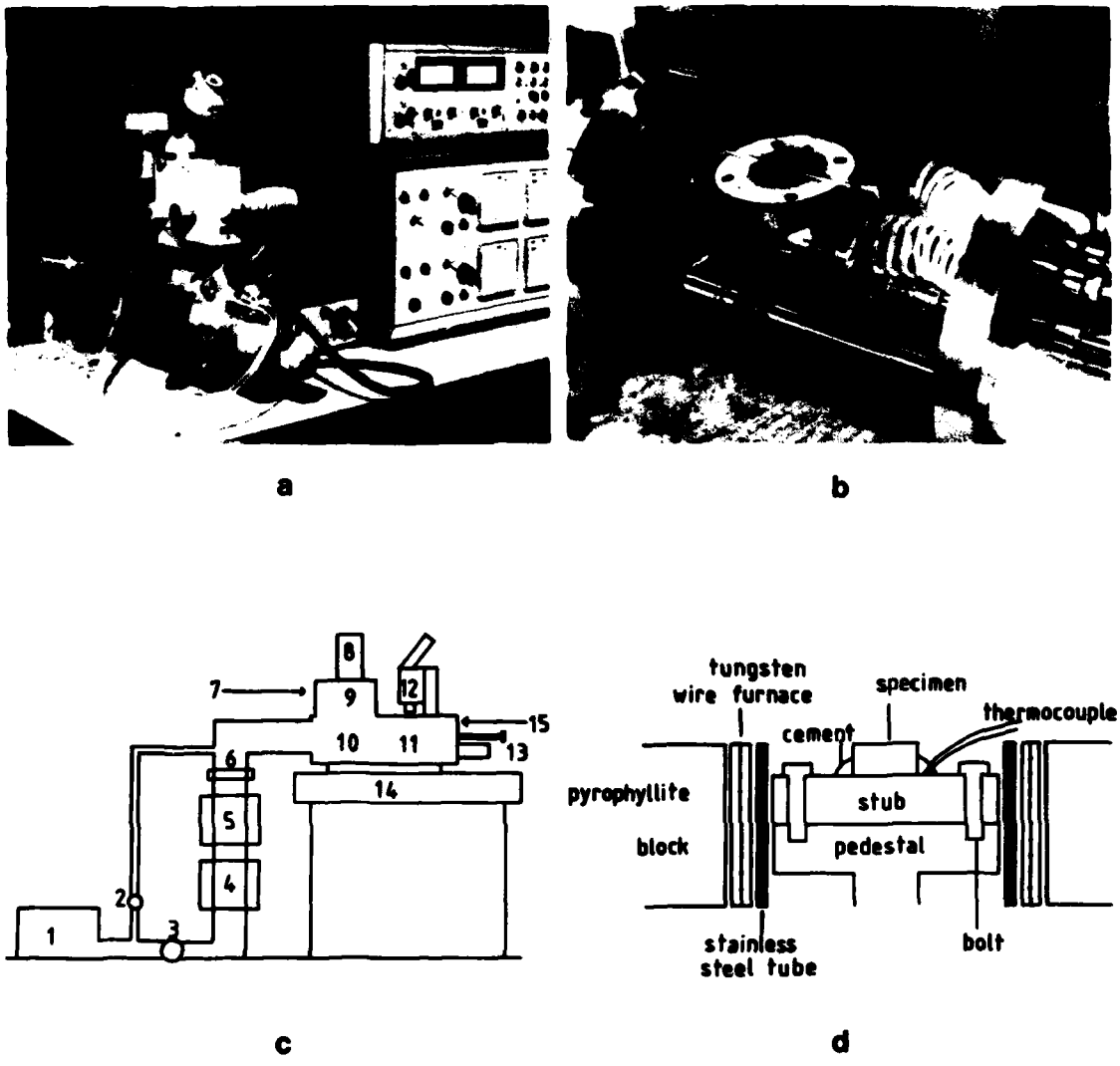

Figure 1. The Temperature-Controlled Microhardness Tester. (a) general view showing the control consoles; (b) the specimen furnace assembly; (c) schematic layout of the system (see key below); (d) schematic layout of the specimen furnace assembly. Key: (1) rotary pump, vacuum switch, Pirani head, (2) roughing valve, (3) backing valve, (4) 4" oil diffusion pump, (5) liquid nitrogen trap, (6) 1/4 swing butterfly valve, Pirani and Penning gauge heads, air inlet valve, (7) gas bleed location (coupled to leak valves), water cooling and electrical feed-throughs to indenter furnace, (8) loading system, (9) indenter plus heater assembly with external dashpot, (10) specimen furnace assembly in the 'indent' position, (11) specimen furnace assembly in the 'view' position beneath the quartz window, (12) microscope with long working distance objective, (13) specimen traverse/rotate controls, (14) concrete bench, (15) water cooling and electrical inlets to specimen furnace.

6. RESULTS

6.1 TEMPERATURE AND LOAD DEPENDENCE OF HARDNESS

The variations of Knoop hardness number (KHN) and Vickers hardness number (VHN) (in each case at 1 kgf applied load) with temperature are shown in figures 2 and 3 respectively, and discussed in section 7. Generally, the Knoop data for the four carbides showed a marked decrease in hardness (by a factor of $\sim$2) over the temperature range investigated ($\sim 0.1T_m$- $0.35\ T_m$ for SiC). The form of the graphs is linear except around the 20-200°C range, where a distinct plateau occurred in the cases of (0001) single crystal SiC, sintered SiC and possibly reaction-bonded SiC, although definitely not for hot-pressed SiC. For comparison, the Knoop microhardness of the single crystal measured at room temperature in air was 2410 (±40) $kgfmm^{-2}$ compared with 2370 (20) $kgfmm^{-2}$ measured at $2x10^{-6}$ mmHg, the difference being statistically insignificant.

Vickers hardness data for the carbides showed a more marked decrease (by a factor of $\sim$3) over the same temperature range, the graphs being linear, with no plateau, in all cases (N.B. the reaction-bonded material used for Vickers hardness measurements was from a different fabrication sequence to that used for Knoop measurements, so direct comparison may be unreliable). PDSN showed a much smaller decrease in Vickers hardness over the temperature range (which is $\sim 0.15\text{-}0.5T_m$ for Si_3N_4), the decrease being linear.

The variation of hardness with load (the load sensitivity or indentation size effect (18)) was also investigated as a function of temperature, this being quantified by the Meyer index (n) defined by (20) -

$$P = Ka^n \qquad K = \text{constant}$$

A value of n=2 indicates no variation of hardness with load, while for $n<2$ the hardness decreases with increasing load (see tables 3 (Knoop) and 4 (Vickers)). The variation of n with temperature was similar for all materials, varying from $\sim$1.7 (Knoop) or 1.8-1.9 (Vickers) at room temperature to 1.8-1.9 (Knoop) or 1.9-2.0 (Vickers) at 800°C. One exception appeared to be the (0001) single crystal SiC, which showed an anomalously low value of n (1.5) for 800°C Knoop indentations, but no difference between room temperature and 800°C values in the Vickers case. For the other materials, the slight increases in Meyer index values at high temperatures indicate that the indentation size effect lessens with increasing temperature.

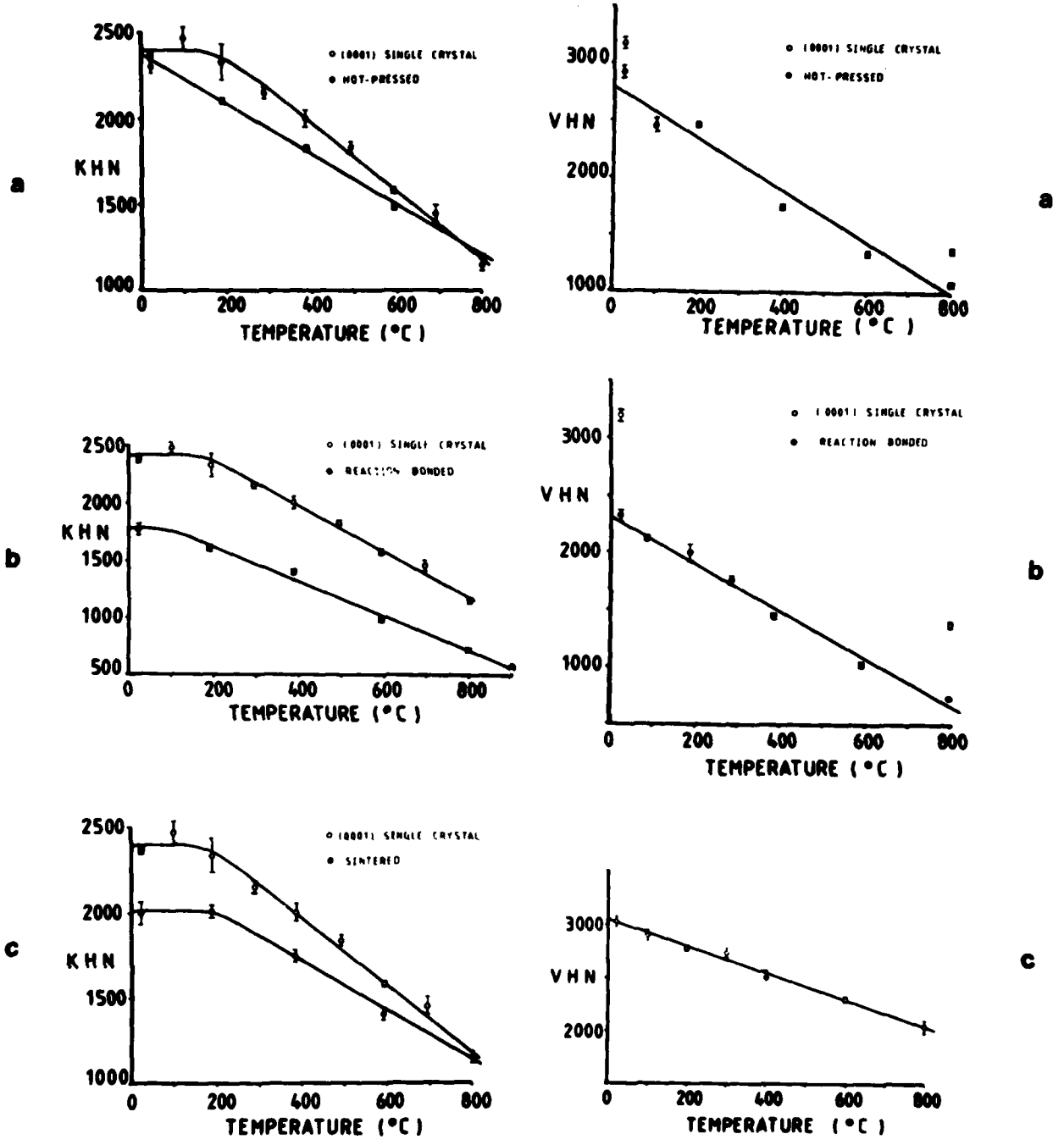

Figure 2. Variation of Knoop Hardness Number (KHN-kgf/mm^{-2}) with temperature for four different microstructural forms of SiC: (0001) single crystal with long indenter axis along <11$\bar{2}$0> and (a) hot-pressed, (b) reaction-bonded and (c) sintered silicon carbides.

Figure 3. Variation of Vickers Hardness Number (VHN-kgf/mm^{-2}) with temperature for three different microstructural forms of SiC ((a) and (b)) and PDSN (c).

Applied load = 1 kgf in all cases. Error bars indicate one standard error in the mean calculated over 5 indentations.

LOAD VARIATION OF KNOOP HARDNESS OF SiC

TEMP. (°C)	SC	HP	S	RB
Room T.	1.75	1.70	1.69	1.69
200	1.68	1.72	1.64	1.65
400	1.71	1.75	1.71	1.63
600	1.71	1.77	1.63	1.65
800	1.53	1.80	1.87	1.79

Table 3. Variation of Meyer Index (n) with temperature for Knoop indentations. Standard errors were typically ±0.03. SC = single crystal SiC, HP = hot-pressed SiC, S = sintered SiC, RB = reaction-bonded SiC.

LOAD VARIATION OF VICKERS HARDNESS OF SiC and Si_3N_4

	SiC			Si_3N_4
TEMP. (°C)	SC	HP	RB	PDSN
Room T.	1.93	1.88	1.80	1.78
200	-	1.96	1.87	1.77
400	-	1.88	1.89	1.85
600	-	1.86	1.99	1.89
800	1.92	1.99	1.91	2.05

Table 4. Variation of Meyer Index (n) with temperature for Vickers indentations. Standard errors were typically ±0.03. SC = single crystal SiC, HP = hot-pressed SiC, RB = reaction-bonded SiC, PDSN = pyrolytically-deposited silicon nitride.

6.2 INDENTATION FRACTURE

A general observation is that all the materials examined showed an increase in the extent of indentation fracture with increasing temperature.

For the (0001) single crystal SiC, room temperature Knoop indentations were often uncracked but sometimes showed lateral vents, particularly where an indentation intersected an obvious flaw such as a surface scratch (fig. 4a). On increasing the temperature, both the incidence and extent of lateral cracking increased dramatically above about 400°C until, by 800°C, almost all the 500g indentations had large lateral vents associated with them (fig. 4b), even 100g indentations often being badly cracked (N.B. subsurface fracture, seen optically as in figs. 4e and f, was always observed beneath indentations showing little surface cracking at high temperatures). Vickers indentations showed predominantly radial fracture (parallel to $\langle 11\bar{2}0 \rangle$ and, to a lesser extent, $\langle 10\bar{1}0 \rangle$ directions), with subsurface lateral fracture visible optically, especially when viewed in reflection between crossed polars (figs. 4e and f). The extent of fracture was again observed to increase with increasing temperature, this being reflected in a decrease in K_c (table 5).

In the hot-pressed SiC, all room temperature indentations showed small amounts of fracture around the indentation profile (figs 5a and d), this being largely lateral in the Knoop case, with both radial and often lateral fracture in the Vickers case. Lateral fracture took the form of a network of small, largely intergranular cracks and chips, the extent of this type of fracture increasing with temperature, becoming quite severe by 800°C (figs. 5b and c), but remaining largely intergranular. Radial fracture became more extensive with increasing temperature up to ∿400°C, remaining constant above this temperature (fig. 9a). Figure 5f shows the existence of slip steps around a 1000gf Vickers indentation made at 800°C.

Reaction-bonded SiC showed some non-extensive indentation fracture at room temperature (figs. 6a and b), the only consistently preferred fracture paths being SiC: Si interfaces (in confirmation of Page et al. (6)) with very occasional grain boundary failure (fig. 6b). Both grades of material (a and b - see table 2) showed similar behaviour in this respect, Vickers indentations showing both lateral and radial fracture, Knoop indentations showing mainly lateral cracks. Unfortunately, Vickers indentations in sample (b) were obscured by material (originating from another part of the furnace assembly) depositing on the specimen surface at 1000°C, so no micrographs of this material are as yet available. Fracture again became more pronounced with increasing temperature (fig. 6), especially around the SiC: Si boundaries, but the effect was not as marked as with the single crystal. Figures 6e and f show possible slip steps in a number of grains immediately adjacent to a 1000gf Knoop indentation made at 900°C.

The sintered SiC showed much less susceptibility to fracture around Knoop indentations than the other materials, room temperature fracture being seldom observed, and limited to areas immediately adjacent to the indentation profile. The incidence of cracking increased slightly with increasing temperature, but not as severely as in the preceding cases (fig. 7). Although the fracture was not extensive, it appeared to be

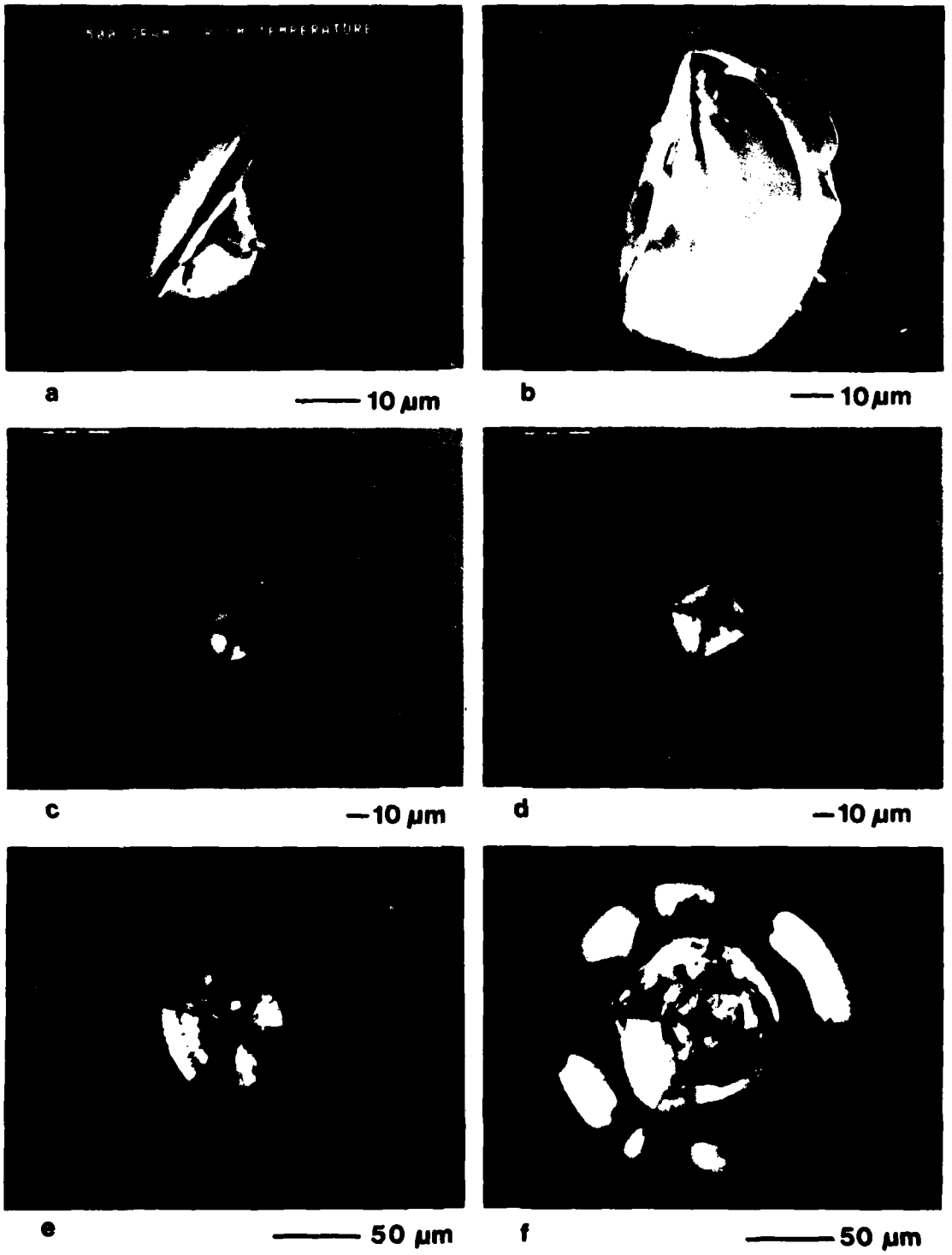

Figure 4. Fracture around Knoop and Vickers indentations in a SiC single crystal (0001) surface with one indenter axis (long diagonal in the Knoop case) parallel to <11$\bar{2}$0> (500gf (Knoop) and 1000gf (Vickers) loads; optical and SEM (secondary) micrographs). (a) Room temperature Knoop indentation showing a small lateral crack associated with a scratch (SEM, 40kV); (b) 800°C indentation showing massive multiple lateral fracture (SEM, 30kV), (c) room temperature Vickers indentation showing radial fracture along <11$\bar{2}$0> and <10$\bar{1}$0> directions and a dark 'halo' around the indentation presumed due to sub-surface lateral fracture of the same extent as the radial cracks (SEM, 40kV); (d) 800°C Vickers indentation showing much more extensive radial fracture along <11$\bar{2}$0> and <10$\bar{1}$0> and faint 'halo' contrast as in (c) (SEM, 40kV); (e) as (c) optical micrograph (crossed polars) showing sub-surface lateral and radial cracks; (f) as (d) optical micrograph (crossed polars) showing much more extensive surface and sub-surface fracture.

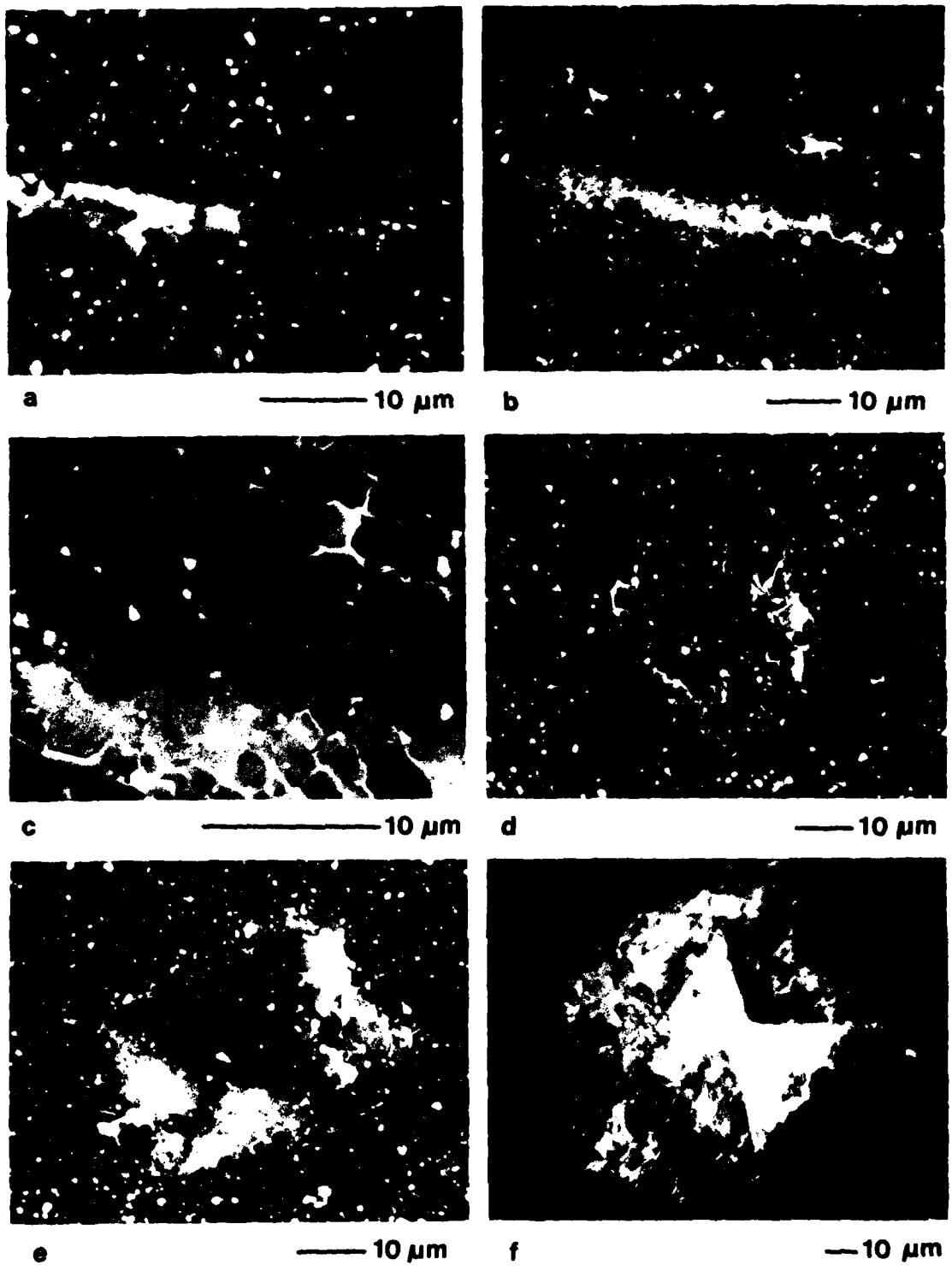

Figure 5. Fracture around Knoop and Vickers indentations in hot-pressed SiC (1000gf load; optical and SEM (secondary) micrographs). Note the specular white intergranular contrast (WC particles - see text) and faint intergranular contrast (presumed due to impurity variations). (a) SEM micrograph (30kV) of a room temperature Knoop indentation displaying distinct intergranular cracking with whole-grain chips; (b) SEM micrograph (30kV) of an 800°C Knoop indentation showing extensive networks of intergranular lateral cracks; (c) as (b); (d) SEM micrograph (40kV) of a room temperature Vickers indentation showing radial and lateral fracture; (e) SEM micrograph (40kV) of an 800°C Vickers indentation showing more extensive fracture; (f) as (e) optical micrograph (Nomarski differential interference contrast) showing slip steps in several grains and surface rumpling of grains adjacent to the indentation.

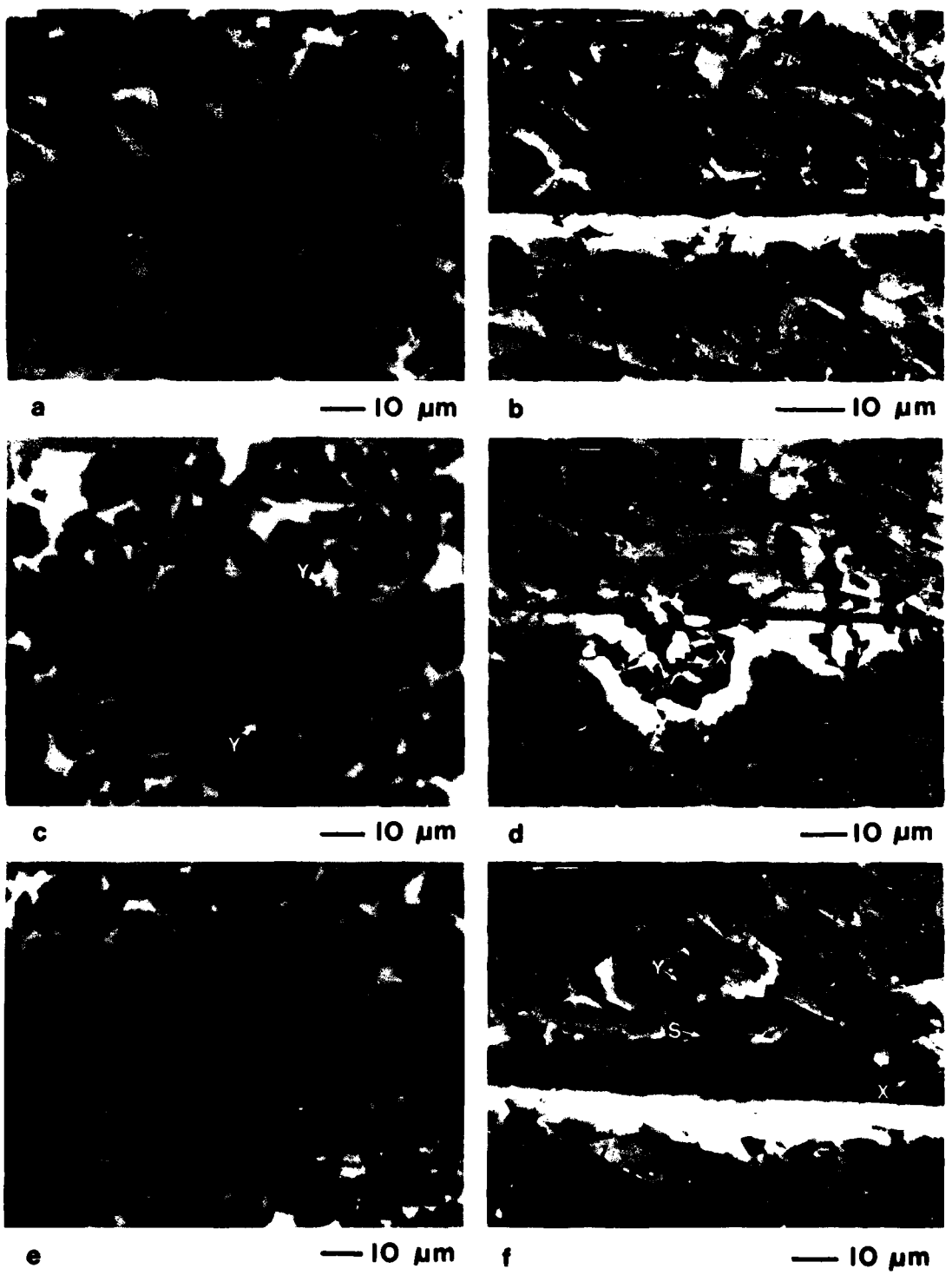

Figure 6. Fracture around Knoop indentations in reaction-bonded (REFEL) SiC (1000gf load; optical and SEM (secondary 30kV) micrographs). (a) Optical micrograph showing limited cracking associated with a room temperature indentation; (b) SEM image of the same indentation showing that some of the fracture is intergranular; (c), (d) optical and SEM micrographs of 400°C indentation showing extensive lateral chipping, much of which is intragranular (note the purity contrast on the fracture facets (X)), or along Si:SiC boundaries (Y); (e) optical micrograph of a 900°C indentation exhibiting extensive networks of cracks predominantly along Si:SiC interfaces. Striations in occasional grains (e.g. S) are attributed to massive slip steps; (f) SEM image of a 900°C indentation showing both inter - (X) and intragranular (Y) cracking with occasional slip steps (S).

intergranular and often associated with pores in the material.

Vickers indentations in PDSN showed extensive (at 1000gf load), well-defined radial cracks at all temperatures, the extent increasing with temperature (fig. 8). Lateral fracture was infrequent, becoming more noticeable at high temperatures and applied loads. Radial cracks often appeared to be associated with the very small amounts of porosity found to be present in this material.

Viewing the specimen optically between crossed polars revealed both the grain structure and sub-surface indentation fracture (fig. 8c, d). Occasionally, grain boundaries appeared to be preferred fracture paths, however the cracking was for the most part intragranular.

Indentation fracture parameters derived from Vickers radial crack length data obtained at various loads and temperatures (using equations a, b and c in section 3) are plotted in table 5 and figure 9 for (0001) single crystal SiC, hot-pressed SiC and PDSN. The single crystal has lower values of both K_c and P* at 800°C than at room temperature, c* being the same in both cases. (H/K_c), the 'index of brittleness' described by Lawn et al. (41, 42), also remains constant. In contrast, hot-pressed SiC shows a decrease in K_c with increasing temperature which levels out at ∿400°C, whilst P* and c* rise above ∿600°C. PDSN again shows different behaviour: K_c decreases linearly with rising temperature over the whole range, whilst P* and c* both remain approximately constant (within experimental errors, which were relatively large due to the dependence on high powers of K_c and H).

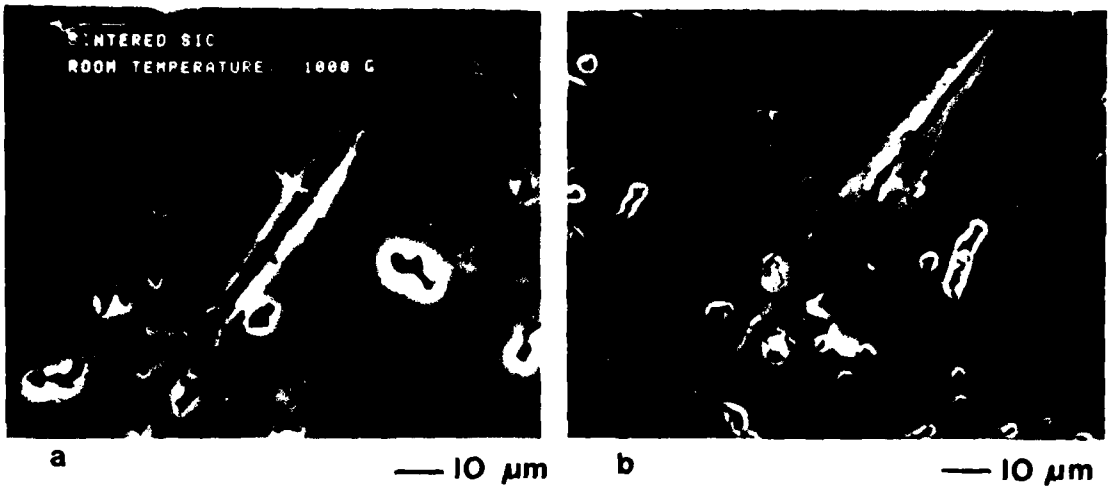

Figure 7. Fracture around Knoop indentations in sintered SiC (1000gf load; SEM (secondary, 30kV) micrographs). (a) Room temperature indentation showing limited cracking around the profile (note the porosity); (b) 800°C indentation exhibiting slightly more extensive cracks which are apparently intergranular and associated with pores.

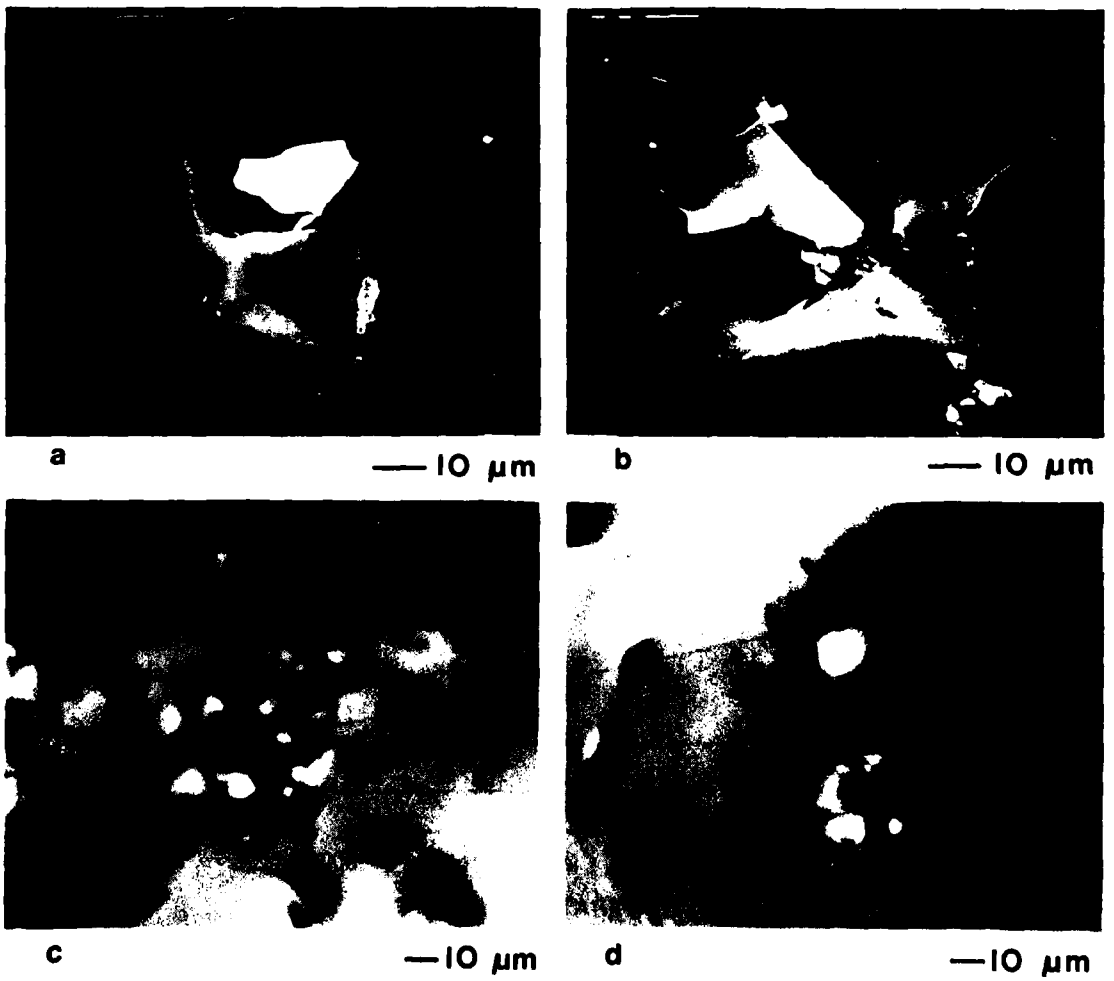

Figure 8. Fracture around Vickers indentations in pyrolytically-deposited Si_3N_4 (1000gf load; optical and SEM (secondary, 40kV, gold sputter-coated specimen) images). (a) SEM image of room temperature indentation showing radial fracture associated with a pore and a lateral vent; (b) SEM image of an 800°C indentation showing more extensive radial and lateral fracture; (c) as (a), optical image (crossed polars) showing surface and sub-surface radial and lateral fracture and orientation-dependent intergranular contrast; (d) as (b), optical image (crossed polars) showing more extensive fracture.

Temperature (°C)	K_C ($MPam^{\frac{1}{2}}$)	$H/K_{C^{\frac{1}{2}}}$ ($\mu m^{\frac{1}{2}}$)	p^* (N)	c^* (μm)
22	4.6(±0.1)	7.7(±0.3)	0.16(±0.03)	2.0(±0.2)
800	2.0(±0.1)	7.8(±0.4)	0.07(±0.01)	2.0(±0.2)

Table 5. Indentation fracture parameters for (0001) single crystal SiC at room temperature and 800°C.

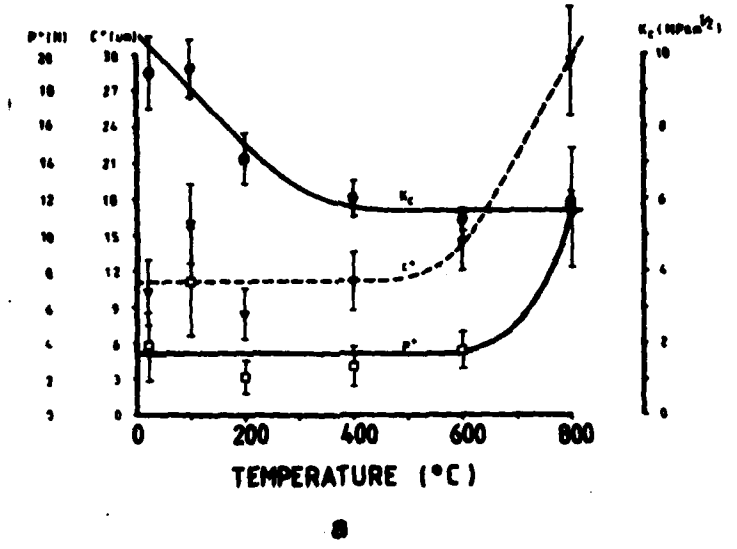

a

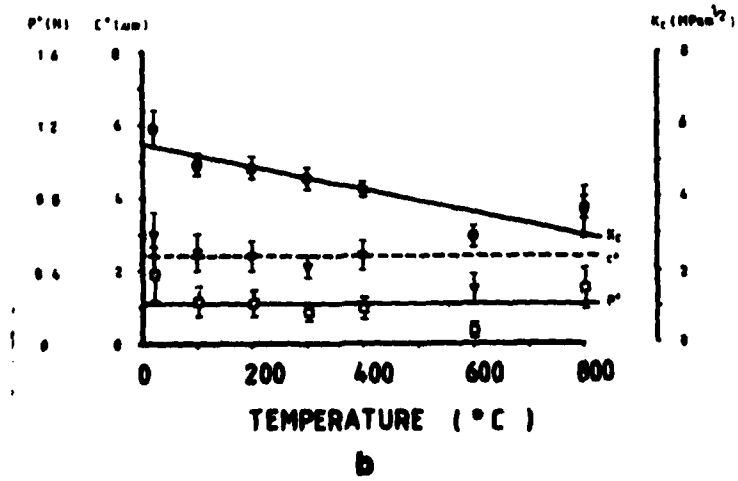

b

Figure 9. Variation of K_C (circles), P^* (squares) and c^* (triangles - broken curves) with temperature for (a) hot-pressed SiC and (b) pyrolytically-deposited Si_3N_4. Error bars indicate one standard error in the mean.

7. DISCUSSION

7.1 HARDNESS AS A FUNCTION OF TEMPERATURE, MICROSTRUCTURE AND LOAD

It has been established that the variation of microhardness with temperature for SiC and Si_3N_4 materials is (a) marked, (b) indenter dependent, (c) material dependent and (d) microstructure dependent. From the data obtained, it is impossible to distinguish between a number of possible mechanisms for the temperature variation of hardness and hence indentation plasticity. Possibilities include (see section 2) the thermal activation of existing slip system(s), the introduction of new ones, the reduced efficiency of dislocation pinning mechanisms (since all materials are impure and charged impurities can greatly affect the slip behaviour of ceramic materials (e.g. 73)), or the increasing effect of indentation creep mechanisms. This latter effect has not been investigated, but is believed not to be extensive for the temperature/indenter dwell times used (59).

From the anisotropy data of Niihara and Hirai (30), there appears to be no activation of new slip systems in the case of Si_3N_4 over this temperature range, similarly the Vickers hardness anisotropy data of Hirai and Niihara (59) indicate that there is probably no activation of new slip systems in SiC (although this matter requires confirmation by more detailed experiments, particularly since Hirai and Niihara observed no hardness plateau, as in the present study). A critical experiment (as yet untried) would be to compare the slip deformation pattern of, say, a room temperature indentation with that associated with one of identical size made at higher temperature with a smaller load. Thus, direct transmission electron microscope observation of deformation structures (e.g. 6,13), together with indirect evidence from etching (74), single crystal hardness anisotropy experiments (e.g. 16,30,59) and possibly selected area electron channelling (14), cathodoluminescence (e.g. 75) or X-ray diffraction techniques will need to be evaluated from a range of samples/temperatures to establish the role of plasticity in the variation of hardness with temperature.

Interestingly, there now exist three independent sets of hot-hardness data for (0001) single crystal SiC (58,59 and the present study) using (fortunately) three different indenters! For the Berkovich profile at 1kgf load, Trefilov et al. found a hardness plateau to occur up to 600°C, followed by a subsequent linear decrease of approx. slope - $5 kgf mm^{-2} K^{-1}$ up to ∿1000°C. The Knoop profile at 1kgf load (reported here) gives a plateau up to ∿200°C followed by a linear decrease of $-1.8 kgf mm^{-2} K^{-1}$ (see also (1)) while the Vickers data of Hirai and Niihara (59) for 100gf load shows no plateau above room temperature but an apparently linear (on a log. hardness plot) decrease corresponding to a slope of $-1.2 kgf mm^{-2} K^{-1}$, (data corrected to 1 kgf standard assuming load variations similar to that found in the present study). The Vickers data from the present study would show a hardness decrease of approx. slope $-2.3 kgf mm^{-2} K^{-1}$ if the variation between 20 and 800°C were linear. However, care must be exercised in comparing the data from different workers, due to possible variations in specimen purity, polytype distribution, etc. Comparison of Vickers and Knoop data for the polycrystalline samples studied here reveals that the Vickers hot-hardness curve is apparently steeper than the Knoop, with the suggestion of a low-temperature plateau region in the Knoop curve, for the reaction-bonded material (a) which is not repeated in the Vickers

case for material (b). No explanation for these differences is yet offered, but it should be recognized that indenter profile will have an effect on both the constraint factor for material flow (19,16) and the precise form of the stress field beneath the indenter.

The hot-hardness results show a difference between the carbide materials and the one form of nitride examined (fig.3): the PDSN sample showed a much less severe decrease in hardness with temperature (from 3000kgfmm^{-2} at room temperature to 2100kgfmm^{-2} at 800°C; c.f. 2800kgfmm^{-2} at room temperature to 1000kgfmm^{-2} at 800°C for the hot-pressed SiC). Only (0001) single crystal SiC was found to be harder than PDSN at room temperature (N.B. PDSN has been reported to be the hardest form of Si_3N_4 known at room temperature (69)) - at elevated temperatures PDSN was harder than all the other materials investigated. Obviously, more microstructural forms of the nitride must be examined before broad comparisons between SiC and Si_3N_4 materials can be made, but the PDSN hot-hardness curve obtained in this study agrees well with those obtained for α-Si_3N_4 single crystal by Niihara and Hirai (30). However, Atkins and Tabor (51) have measured the mutual hardness of polycrystalline, slightly porous (but otherwise uncharacterized) SiC and Si_3N_4 materials at very high temperature $>0.5T_m$ (which is 1200°C for SiC and 800°C for Si_3N_4), concluding that SiC retains its hardness to higher temperatures than Si_3N_4, although the hardness curves were similar when plotted on a homologous scale (this is not the case for the materials/temperatures investigated here).

Microstructure has been found to have a pronounced effect on the hot-hardness behaviour of SiC (figs. 2 and 3): the (0001) single crystal always appeared hardest (due to one particular, unfavourably-oriented slip system operating everywhere under the indenter (16)), followed by hot-pressed, sintered and reaction-bonded materials respectively - the latter probably being influenced by the high residual silicon content. In comparing the single crystal behaviour with those of the polycrystalline samples (fig. 2), it is immediately apparent that the slopes of the Knoop plots for the hot-pressed and sintered samples are approximately the same and together less than that for the single crystal, such that the hardness of these two samples becomes equal to, then exceeds, that of the single crystal at $\sim$800°C. This effect is presumed due to some form of microstructural slip impedance in the polycrystalline samples, where grain size should be important. Again, it is anticipated that direct investigation of sub-surface deformation patterns may be the only way of resolving the origins of many of the differences in behaviour reported here. The reaction-bonded material exhibited a Vickers hardness/temperature plot similar to the hot-pressed material, but transposed to lower values.

The similarity of the hot-pressed and sintered SiC plots at higher temperatures suggests that porosity in the sintered material is unimportant in determining the hardness and temperature reponse above $\sim$200°C. The low-temperature plateau for sintered SiC may be caused by compaction due to the influence of porosity, in accordance with the ideas of Atkins and co-workers (48, 51, 55, 61) (see section 4), however 200°C is only $\sim$0.15 T_m for SiC, whereas porosity effects have been reported to extend up to $\sim$0.4T_m for other materials (although this value probably depends on the amount and nature of porosity present). Further work is required to clarify this point.

A critical observation is that over the same temperature range as used here, the modulus of rupture (and similar bulk mechanical properties) of all samples shows no significant variation with temperature (for REFEL, for example, the M.O.R. is approximately constant until the silicon melts at ∿1400°C (e.g. 4)) suggesting not only that plasticity plays little or no part in the response to more conventional test situations but that properties such as M.O.R. give little true guide to the type of behaviour (and its temperature sensitivity) prevalent in surface contact situations.

The load dependence of hardness (Knoop and Vickers) is given in tables 3 and 4 for each material. Possible origins of load sensitivity have been discussed (20) but are difficult to determine for any particular material. Specimen microstructure is thought to play a particularly significant role in impeding motion of the extending plastic yield front at increasing loads and it is thus surprising that all the samples studied here should be similar when the microstructures are markedly different. However, the indentation-affected volume is much larger than the expected microstructural scale in all cases except for the PDSN, but more complex statistical analysis is really required to quantify these effects (20). TEM may be the only means of examining this phenomenon further. Again, indenter effects are not understood.

7.2 INDENTATION FRACTURE

As a general prelude, it is emphasized that the extent of cracking (lateral and radial) increased with increasing temperature for all the materials studied. Equation c (section 3) implies that the indentation fracture toughness must therefore decrease with increasing temperature, in contrast with reported (76) bulk mechanical values of K_{IC} which are temperature-insensitive for single-crystal, hot-pressed and reaction-bonded SiC. Since the hardness H also decreases with temperature, the crack initiation parameters P^* and c^* may increase, decrease or remain constant as the ratios (K_c^4/H^3) and $(K_c/H)^2$ respectively change. Physical interpretations of such variations must, however, await a more detailed understanding of indentation fracture initiation mechanisms.

From figure 9 and table 5, hot-pressed SiC shows a higher room temperature value of K_c (∿10MPam$^{\frac{1}{2}}$) than single crystal SiC and PDSN (having values 4.6 and 5.9MPam$^{\frac{1}{2}}$ respectively, c.f. (69): K_c = 3.2MPam$^{\frac{1}{2}}$ for PDSN). This temperature variation of K_c levels off at ∿5.7MPam$^{\frac{1}{2}}$ above ∿400°C for hot-pressed SiC, whilst PDSN appears to show a linear decrease over the whole range, such that K_c∿3MPam$^{\frac{1}{2}}$ at 800°C. Single crystal SiC also shows a decrease in K_c with temperature, although the precise form of the decrease was not determined.

The increase in the extent of crack propagation with temperature is associated with increasing plasticity, as witnessed by both the decrease in hardness and the appearance of slip lines formed around high-temperature, high-load indentations in hot-pressed and reaction-bonded SiC materials (see also 59). The effects of the plastic zone on indentation fracture have been discussed in section 3, and it would be instructive to obtain data on the temperature dependence of Young's modulus for the materials examined, with a view to incorporating the $(E/H)^{2/5}$ term discussed by Evans (80), particularly since the loads used in the present analysis were relatively low (although $P_{oc}^{3/2}$ was verified). In polycrystalline samples, the effects of increasing temperature on grain

boundary cohesion (discussed later) must be determined - increased temperature may result in easier grain boundary crack propagation. The crack initiation parameters were also found to vary with temperature: for hot-pressed SiC at room temperature, P* (~4 N) and c* (~10μm) were substantially higher than corresponding values for PDSN (0.4 N and 3μm) indicating that hot-pressed SiC has a higher resistance to initiation of fracture. This became even more marked above 600°C, at which point the P* and c* curves rose for hot-pressed SiC, remaining constant over the whole temperature range in the case of PDSN, thus maintaining a high susceptibility to both initiation and propagation of cracks. The (0001) single crystal SiC showed a decrease in P* between 20°C (P* = 0.16 N) and 800°C (P* = 0.07 N) with c* remaining constant at 2μm. The effects of temperature on the nucleation parameters are also not well understood and some possible factors are listed but will require further investigation:

i) as the plastic zone depth increases with increasing temperature, the point of maximum tensile stress on the load axis (at the elastic/plastic zone boundary) samples more volume of material for pre-existing flaws and this would result in a decrease in P*;

ii) if nucleation is controlled by plasticity mechanisms, it should be facilitated at higher temperatures, again resulting in a decrease in P* (c* being irrelevant);

iii) higher temperatures may anneal out surface flaws, which would result in increased values of P*;

iv) different crack nucleation mechanisms may operate at higher temperatures (e.g. grain boundary sliding in materials with boundary phases which soften at higher temperatures). The study of preferred fracture paths with regard to specimen microstructure thus becomes of great importance in understanding both crack propagation and nucleation.

Preferred lateral fracture paths in the single crystal SiC often appeared to be associated with (0001) cleavage, confirming the observations of Adewoye (7), who showed that even general conchoidal fracture surfaces through single crystals could be resolved into a series of cleavage steps. Radial fracture around Vickers indentations was parallel to $\langle 11\bar{2}0 \rangle$ and, to a lesser extent $\langle 10\bar{1}0 \rangle$ directions. N.B. Knoop indenter profiles generally promote lateral cracking, whereas Vickers indentations show largely radial fracture, thus a combination of indentation techniques may be used to completely characterize indentation fracture behaviour.

For hot-pressed SiC, the increasing incidence of grain boundary fracture with temperature suggests both a low value of grain boundary cohesive energy and also some probable dramatic changes in grain boundary behaviour (at temperatures still well below those demanded in many proposed applications for these materials), presumably due to thin (~20Å) glassy films postulated and recently directly observed in hot-pressed ceramics (e.g. 77). However, detailed HREM studies will be needed to investigate this further.

Reaction-bonded SiC displayed preferred fracture along SiC: Si interfaces, with other cracks often being transgranular rather than

along grain boundaries. This behaviour persisted with increasing temperature and the apparent fracture resistance of grain boundaries in this material is of great structural interest.

By comparison, the sintered SiC exhibited less indentation fracture which otherwise appeared to be either nucleated or arrested (or both) by porosity in the microstructure. However, the limited extent of the fracture has, as yet, precluded any study of preferred fracture paths in this material. Vickers indentation experiments are also planned for this material. Again, the relatively fracture-resistant grain boundaries in this sample are worthy of further HREM investigation.

PDSN formed well-defined radial cracks around Vickers indentations at all temperatures, the fracture being associated with porosity as in the case of sintered SiC, and largely intragranular in nature (probably facilitated by the large grain size of the material).

8. CONCLUSIONS

Temperature- and load-variable microhardness tests have been used to study the changing incidence of plasticity and fracture, particularly the microstructural control of fracture paths and the parameters influencing crack propagation (K_C) and initiation (P^* and c^*) in a number of different forms of SiC and one form of Si_3N_4 ceramic materials. The observed behaviour, in terms of increasing temperature resulting in decreasing hardness, increasing plasticity and increasing extent of indentation fracture, is of direct relevance to both abrasion - and erosion-resistant applications of these materials. However, in many cases the fundamental origins of the materials' behaviour require continued investigation for full identification. It is also apparent that the results of indentation tests are more useful than bulk mechanical properties as guides for materials selection for surface-contact applications.

9. FURTHER WORK

The following topics for investigation are considered crucial in further understanding the effects of temperature on surface contact phenomena in SiC and Si_3N_4 materials:

- examination of the temperature response of indentation plasticity as revealed by single crystal hardness anisotropy experiments and techniques such as HREM, chemical etching, electron channelling, cathodoluminescence, X-ray diffraction, etc. to determine the nature and extent of slip beneath an indenter;

- further investigation of the effects of specimen microstructure on plasticity and especially fracture processes (by examination of as wide a range of materials as possible);

- indentation creep effects (the dependence of indentation size on indenter dwell time);

- chemomechanical effects (examined by changing the gaseous environment around the specimen);

- determination of the extent to which dynamic situations (e.g. abrasive wear, erosion) reflect the changes in materials response measured by quasi-static indentation techniques. This may be studied by, for example, sliding stylus experiments performed under identical conditions of temperature, environment and applied load as the corresponding quasi-static hardness tests.

10. ACKNOWLEDGEMENTS

The European Research Office of the U.S. Army is gratefully acknowledged for support and sponsorship. Thanks are also due to Professor R.W.K.Honeycombe for the provision of laboratory facilities and to S.R.C. for funding of the hot-hardness tester. We would also like to thank Dr. R.N. Katz (AMMRC, Watertown, USA), Mr. P. Kennedy (UKAEA, Springfields, UK) and Dr. D.J. Godfrey (Admiralty Marine Technology Establishment, Holton Heath) for supplies of specimen material and Messrs. D. Ackland, B. Barber and Ms. V. Kohler for various technical assistance, Mrs. E. Palmer kindly typed the manuscript. Finally, thanks are due to Dr. K. Gove (Wilberforce Scientific Developments Ltd.) for advice and co-operation concerning the construction of the hardness tester.

11. REFERENCES

1. Naylor, M.G.S. and Page, T.F., 1979, Proceedings of the Fifth International Conference on Erosion by Liquid and Solid Impact (ELSI V), 3-6th September, 1979, Newnham College, Cambridge. (Publ. R.A.E. Farnborough), 32.

2. Burke, J.J., Gorum, A.E. and Katz, R.N., 1974, "Ceramics for High Performance Applications" (Army Materials Technology Conference Series), Brook Hill.

3. Katz, R.N., 1980, Proceedings of the Third International Conference on Mechanical Behaviour of Materials, 20th August 1979, Volume 1, Eds. Miller, K.J. and Smith, R.F., Pergamon Press (to be published).

4. Kennedy, P. and Shennan, J.V., 1973, Atom (No. 206), 260.

5. "Silicon Nitride as a Bearing Material". Program Review: U.S. Naval Air Systems Command and U.S. Office of Naval Research, July, 1974. (Proc. of a meeting held at SKF, King of Prussia, Pa. 9-10 July, 1974).

6. Page, T.F., Sawyer, G.R., Adewoye, O.O. and Wert, J.J., 1978, Proc. Brit. Ceram. Soc. 26, 193.

7. Adewoye, O.O., 1976, Ph.D. Thesis, University of Cambridge.

8. Sawyer, G.R., 1979, Ph.D. Thesis, University of Cambridge.

9. Naylor, M.G.S., 1978, M.Phil. Thesis, University of Cambridge, Department of Metallurgy and Materials Science.

10. Hockey, B.J., Wiederhorn, S.M., 1979, Proceedings of the Fifth International Conference on Erosion by Liquid and Solid Impact (ELSI V),3-6th September, 1979, Newnham College, Cambridge. (Publ. R.A.E. Farnborough), 26.

11. Evans, A.G., Gulden, M.E. and Rosenblatt, M., 1978, Proc. Roy. Soc. Lond. A361, 343.

12. Hockey, B.J. and Lawn, B.R., 1975, J. Mater. Sci. 10, 1275.

13. Hockey, B.J., Wiederhorn, S.M. and Johnson, H., 1978, in 'Fracture Mechanics of Ceramics 3', (Eds. Bradt, R.C., Hasselman, D.P.H. and Lange, F.F.), Plenum Press, p.379.

14. Lankford, J. and Davidson, D.L., 1979, J. Mater. Sci. 14, 1669.

15. Ruff, A.W. and Wiederhorn, S.M., 1979, in 'Treatise on Materials Science and Technology, Vol. 16, Materials Erosion' (Ed. C.M. Preece), Academic Press, Chpt. 2.

16. Sawyer, G.R., Sargent, P.M. and Page, T.F., 1980, J. Mater. Sci. (to be published).

17. Van Vechten, J.A., 1973, Phys. Rev. B7, 1479.

18. Sargent, P.M., 1979, Ph.D. Thesis, University of Cambridge.

19. Brookes, C.A., O'Neill,J.B. and Redfern, B.A.W., 1971, Proc. Roy. Soc. Lond. A322, 73.

20. Sargent, P.M. and Page, T.F., 1978, Proc. Brit. Ceram. Soc. 26, 209.

21. Marsh, D.M., 1964, Proc. Roy. Soc. Lond. A279, 420.

22. Johnson, K.L., 1970, J. Mech. Phys. Sol. 18, 115.

23. Studman, C.J., Moore, M.A. and Jones, S.E., 1977, J. Phys. D. 10, 949.

24. Brookes, C.A. and Burnand, R.P., 1971, in 'The Science of Hardness Testing and Its Research Applications', (Eds. Westbrook, J.H. and Conrad, H.), American Society for Metals, p.199.

25. Morgan, G. and Lewis, M.H., 1974, J. Mater. Sci. 9, 349.

26. Rowcliffe, D.J. and Hollox, G.E., 1971, J. Mater. Sci. 6, 1261.

27. Idem.,ibid., 6, 1270.

28. Kumashiro, Y. Itoh,A., Kinoshita, T. and Sobajima, M., 1977, J. Mater. Sci. 12, 595.

29. Shaffer, P.T.B., 1964, J. Amer. Ceram. Soc. 47, 466.

30. Niihara, K. and Hirai, T., 1979, J. Mater. Sci. 14, 1952.

31. Hagan, J.T., 1979, J. Mater. Sci. 14, 2975.

32. Lawn, B.R. and Wilshaw, T.R., 1975, J. Mater. Sci. 10, 1049.

33. Lawn, B.R. and Swain, M.V., 1975, J. Mater. Sci. 10, 113.

34. Lawn, B.R. and Fuller, E.R., 1975, J. Mater. Sci. 10, 2016.

35. Evans, A.G. and Wilshaw, T.R., 1976, Acta. Metall. 24, 939.

36. Swain, M.V. and Hagan, J.T., 1976, J. Phys. D. 9, 2201.

37. Hagan, J.T., 1979, J. Mater. Sci. 14, 462.

38. Perrott, C.M., 1977, Wear 45, 293.

39. Moore, M.A., 1979, Proc. Int. Conf. 'Wear of Materials', Dearborn, Michigan, April 16-18, 1979, (Eds. Luderna, K.C., Glaeser, W.A. and Rhee, S.K.), p.275.

40. Lawn, B.R., Jensen, T. and Arora, A., 1976, J. Mater. Sci. 11, 573.

41. Lawn, B.R. and Evans, A.G., 1977, J. Mater. Sci. 12, 2195.

42. Lawn, B.R. and Marshall, D.B. 1979, J. Am. Ceram. Soc. 62, 347.

43. Lankford,J., Davidson, D.L., 1979, J. Mater. Sci. 14, 1662.

44. Lawn, B.R. and Marshall, D.B., 1978, in 'Fracture Mechanics of Ceramics 3', (Eds. Bradt, R.C., Hasselman, D.P.H. and Lange, F.F.), Plenum Press, p.205.

45. Gove, K.B. and Charles, J.A., 1974, Metals Technology, 1, (6), 279.

46. Gove, K.B. and Charles, J.A., 1974, Met. Sci. J. 8, 367.

47. Marchant, H.D., Murty, G.S., Bahadur, S.N. and Mehrotra, Y., 1973, J. Mater. Sci. 8, 437.

48. Atkins, A.G., 1971, in 'The Science of Hardness Testing and its Research Applications' (Eds. Westbrook, J.H. and Conrad, H.), American Society for Metals, p.223.

49. Tokar, M. and Green, J.L., 1971, ibid., p.241.

50. Loladze, T.N., Bokuchava, G.V. and Davidova, G.E., 1971, ibid., p. 251.

51. Atkins, A.G. and Tabor, D., 1966, Proc. Roy. Soc. Lond. A292, 441.

52. Atkins, A.G., Silverio, A. and Tabor, D., 1966, J. Inst. Metals, 94, 369.

53. Tarkanian, M.L., Neumann, J.P. and Raymond, L., 1971, in 'The Science of Hardness Testing and its Research Applications', (Eds. Westbrook, J.H., and Conrad, H.), American Society for Metals, p.187.

54. O'Neill, J.B., Redfern, B.A.W. and Brookes, C.A., 1973, J. Mater. Sci. 8, 47.

55. Fitzgerald , L.M., 1963, J. Less-Common Metals 5, 356.

56. Hannink, R.H.J., Kohlstedt, D.L. and Murray, M.J., 1972, Proc. Roy. Soc. Lond. A326, 409.

57. Kohlstedt, D.L., 1973, J. Mater. Sci. 8, 777.

58. Trefilov, V.I., Borisenko, V.A., Gnesin, G.G., Gridneva, I.V. and Milman, Iu.V., 1977, Dokl. Akad. Nauk.SSSR, 239, 579. (In Russian).

59. Hirai, T. and Niihara, K., 1979, J. Mater. Sci. 14, 2253.

60. Huseby, I.C. and Petzow, G., 1974, Powder Met. Int. 6, 17.

61. Brookes, C.A. and Atkins, A.G., 1964, Proc. 5th Plansée Seminar, Reutte 1964, Springer-Verlag 1965. p.712.

62. Brookes, C.A., 1962, in 'Special Ceramics 1962' (Ed. P. Popper), British Ceramic Research Association, Ch.11, p.221.

63. Brookes, C.A. and Imai, M., 1964, in 'Special Ceramics 1964' (Ed. P. Popper), British Ceramic Research Association, p.251.

64. Westwood, A.R.C., Goldheim, D.L. and Lye, R.G., 1967, Phil. Mag. 16, 505.

65. Macmillan, N.H., 1977, in 'Surface Effects in Crystal Plasticity' (Ed. Latanision R.M. and Fourie J.T.), Nato Advanced Study Inst. Series (Nordhoff, Leyden), pp.629-661.

66. Verma, A.R. and Krishma, P., 1966, 'Polymorphism and Polytypism in Crystals', J. Wiley Inc., p.93.

67. Smith, D.J., Jepps, N.W. and Page, T.F., 1978, J.Microscopy,114,1.

68. Edmonds, A.J.S., 1979, Ph.D. Thesis, University of Cambridge.

69. Pitman, K.C. and Godfrey, D.J., 1978, Proc. Brit. Ceram. Soc. 26, 225.

70. Sawyer, G.R. and Page, T.F., 1978, J. Mater. Sci. 13, 885.

71. Burnett, P.J., Naylor, M.G.S. and Page, T.F., 1979, unpublished research.

72. Cassidy, J.E., 1977, Bull. Am. Ceram. Soc. 56, No. 7, 640.

73. Plekta, B.J., Mitchell, T.E. and Heuer, A.H., 1975, in 'Deformation of Ceramic Materials', (Eds. Bradt, R.C. and Tressler, R.E.), Plenum Press, p.181.

74. Adewoye, O.O. and Page, T.F., 1976, J. Mater. Sci. 11, 981.

75. Chin, A.K., Mahajan, S. and Ballman, A.A., 1979, Appl. Phys. Lett. 35, (10), 784.

76. Henshall, J.L., 1975, Ph.D. Thesis, University of Cambridge.

77. Clarke, R.D. and Thomas, G., 1978, J. Am. Ceram. Soc. 61, 114.

78. Hill, R., 1950, 'The Mathematical Theory of Plasticity', (Clarendon Press, Oxford).

79. Hagan, J.T. and Swain, M.V., 1978, J. Phys. D. 11, 2091.

80. Evans, A.G., 1980, unpublished work.

81. Jepps, N.W. and Page, T.F., 1979, J. Microscopy, 116, 159.

82. Adewoye, O.O., Sawyer, G.R., Edington, J.W. and Page, T.F., 1974, Technical Report to U.S. Army (AMMRC), October 1974, Contract No. DAJA37-74-C-1310.

83. Moulson, A.J., 1979, J. Mater. Sci., 14, 1017.

84. Edington, J.W., Rowcliffe, D.J. and Henshall, J.L., 1975, Powder Met. Int. 7, No. 2., 82.

12. GLOSSARY

T_m = absolute melting point

KHN = Knoop Hardness Number ($kgfmm^{-2}$)

VHN = Vickers Hardness Number ($kgfmm^{-2}$)

a = indentation diagonal radius

c = median/radial crack radius

P = applied load

K_c = indentation fracture toughness (K_{IC})

P* = minimum load required to cause a crack nucleus (c>c*) to grow

c* = minimum size of crack nucleus which may propagate (at P>P*)

β_o = constant

λ_o = constant

μ_o = constant

E = Young's modulus